

## Research Article

# Random-Access Technique for Self-Organization of 5G Millimeter-Wave Cellular Communications

Jasper Meynard Arana, Joo Pyo Han, and Yong Soo Cho

*School of Electrical and Electronics Engineering, Chung-Ang University, Seoul, Republic of Korea*

Correspondence should be addressed to Yong Soo Cho; yscho@cau.ac.kr

Received 17 June 2016; Accepted 7 August 2016

Academic Editor: Hyun-Ho Choi

Copyright © 2016 Jasper Meynard Arana et al. This is an open access article distributed under the Creative Commons Attribution License, which permits unrestricted use, distribution, and reproduction in any medium, provided the original work is properly cited.

The random-access (RA) technique is a key procedure in cellular networks and self-organizing networks (SONs), but the overall processing time of this technique in millimeter-wave (mm-wave) cellular systems with directional beams is very long because RA preambles (RAPs) should be transmitted in all directions of Tx and Rx beams. In this paper, two different types of preambles (RAP-1 and RAP-2) are proposed to reduce the processing time in the RA stage. After analyzing the correlation property, false-alarm probability, and detection probability of the proposed RAPs, we perform simulations to show that the RAP-2 is suitable for RA in mm-wave cellular systems with directional beams because of the smaller processing time and high detection probability in multiuser environments.

## 1. Introduction

As the demand for capacity in mobile broadband communications increases drastically every year, wireless communication industries are preparing to support up to a thousandfold increase in total mobile traffic by 2020 [1–3]. Millimeter-wave (mm-wave) communications with possible multigigabit-per-second data rates have attracted much attention as a candidate technology for the 5G era [4, 5]. Highly directional beamforming antennas are necessary at both the base station (BS) and mobile station (MS) to compensate for the high attenuation in the mm-wave frequency band and to extend its transmission range. With the small wavelength corresponding to mm-wave frequencies, antenna arrays can be easily installed in the MS.

A misalignment between transmit (Tx) and receive (Rx) beams may cause a significant loss in the received power, especially for systems with narrow beams. Beam alignment in mm-wave communication systems is necessary to find the best beam pair from all possible beam pairs for maximum beamforming efficiency. Currently, switched beamforming techniques with a set of predefined angles are used for Tx-Rx beamforming because the multiple analog chains at mm-wave frequencies are costly, and sampling analog signals at

GHz rates consumes a substantial amount of power [6]. The best beam pair is determined by selecting a beam pair with the maximum array gain. The Tx-Rx beamforming technique using the 60 GHz unlicensed spectrum with a bandwidth of 2.16 GHz has already been standardized in IEEE 802.11ad to provide multigigabit-per-second data rates [7]. However, the standard is mainly designed for indoor communications (wireless LAN) and is not adequate for cellular communication.

Random access (RA) is a key procedure in cellular networks, enabling an MS to initiate communications and time alignment to a BS. RA is also one of the key procedures in self-organizing networks (SONs) [4]. In [8], a RA procedure for mm-wave cellular systems is described, where preambles are transmitted/received repeatedly in multiple directions from the MS/BS. Individual Tx beams are transmitted by the MS until all of the Tx beams are transmitted. The Rx beam sweep is performed at the BS for each Tx beam to measure the signal-to-noise ratio (SNR) for every Tx-Rx pair. However, the total RA duration will be very long because the RA preamble (RAP) should be long enough to be detected by the BS in large coverage areas, and multiple preambles should be transmitted for all directions of Tx and Rx beams. In [9], a RA technique with beamforming, referred to as an adaptive

spatial RA, is proposed, where beams are generated depending on the number of MSs and their locations. In this technique, the probability of a collision can be significantly reduced by exploiting the space domain efficiently in the RA stage. However, this technique cannot be employed in mm-wave cellular systems with switched beamforming because a fixed set of predefined angles is used in switched beamforming, and the previous collision statistic is required to adjust the beams in the next frame.

In this paper, we propose a new technique that can reduce the processing time in the RA stage. We design an RAP for mm-wave cellular systems with switched beamforming. Unlike the conventional RA preamble, which carries six bits (a total of 64 preamble IDs), the proposed RA preamble carries the information on beam ID (BID; optimal downlink Tx beam) as well as the preamble ID (PID; one of 64 signatures), all at the physical layer. The preambles are designed such that the additional information on the BID does not affect the number of available PIDs. We propose two different types of preambles (RAP-1 and RAP-2) that satisfy the constant-amplitude zero-autocorrelation (CAZAC) property for RA in mm-wave cellular systems. After analyzing the properties of the proposed preambles, false-alarm and detection probabilities are derived when the proposed preambles are used for RA. Using simulations, we show that the proposed technique can significantly reduce the processing time in the RA stage, and the proposed RAP-2 is appropriate for RA in mm-wave cellular systems with directional beams because it provides high detection probability in multiuser environments.

The remainder of the paper is organized as follows. In Section 2, we discuss an RA procedure for mm-wave cellular systems with directional beams. We propose an RA procedure that can reduce the processing time using the proposed RAP. In Section 3, we propose two different types of RAPs for mm-wave cellular systems and discuss their correlation properties. In Section 4, we describe a detection technique for the proposed RAP and derive the false-alarm probability and detection probability when the proposed RAPs are used for RA. In Section 5, we evaluate the performance of the proposed RA technique by performing computer simulations using a simple model of an mm-wave cellular system after verifying the properties of the proposed RAP. In Section 6, we conclude the paper.

## 2. RA Procedure in mm-Wave Cellular Systems

RA is generally performed when an MS turns on from sleep mode, performs a handover from one cell to another, or loses uplink time synchronization. The RA procedure in Long-Term Evolution (LTE) consists of five steps. In the first step, downlink synchronization and cell searching are performed by receiving synchronization channel and broadcast channel [10]. After acquiring downlink synchronization and receiving system information including information on parameters specific to RA, the MS performs RA preamble transmission in Step 2. The MS selects one of 64 predefined sets of preambles and transmits it using the time-frequency resources indicated by the system information. When the BS successfully receives the RA preamble, it sends a RA response (RAR) indicating

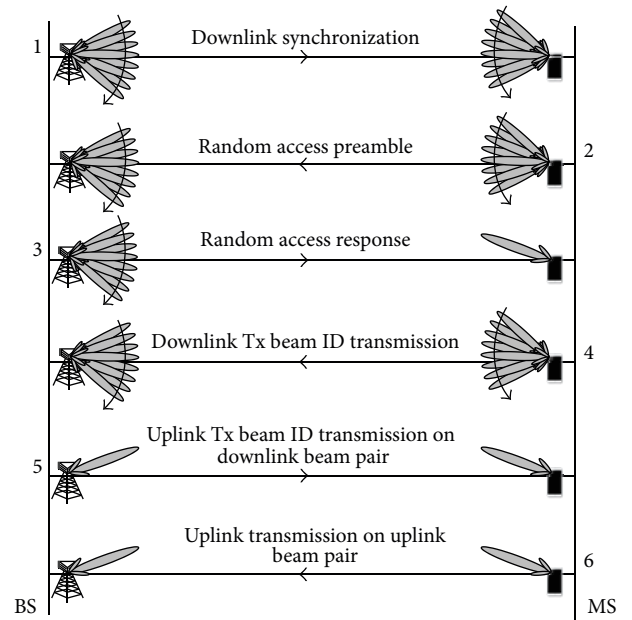


FIGURE 1: Conventional random-access procedure in mm-wave cellular systems.

a preamble index, uplink timing advance (TA), and uplink resource-allocation information in Step 3. The MS can then determine whether its RA attempt has been successful by matching the preamble index. In Step 4, if the preamble index matches, the MS uses the TA information to adjust its uplink timing and transmits a RA message including the MS identity in the resource allocation provided by the previous step. In Step 5, the BS transmits the MS identity to the MS. If the MS cannot decode its own MS identity, it will automatically exit the procedure and resume the RA process.

In mm-wave cellular communication systems with directional beams, the RA procedure needs to be modified because the best beam pair for uplink transmission is unknown in the initial state. Figure 1 shows the initial RA procedure for an LTE-based mm-wave cellular communication system with directional antennas. Hereafter, we refer to this procedure as the conventional RA procedure. Here, we assumed that channel reciprocity does not hold; that is, the best beam pair in the downlink is not the same as the best beam pair in the uplink because of the different characteristics of the RF circuitry of the transmitter and receiver.

The first step starts with the downlink synchronization. The BS transmits synchronization signals, a primary synchronization signal (PSS), and secondary synchronization signal (SSS), for synchronization at the MS [11]. Then, the BS transmits a system information block (SIB) on a physical broadcast channel (PBCH), which carries configuration parameters of physical RA channels (PRACHs) such as the preamble root index. The same signals are transmitted repeatedly in individual beams until all of the Tx and Rx beams are swept, because the best downlink beam pair is not yet known. The MS is synchronized with the BS and determines the best downlink beam pair (downlink Tx beam and Rx beam) in this step. Upon decoding the SIB transmitted on the best downlink

beam pair, the MS will select a preamble signature for RA. In Step 2, the selected preamble signature will be transmitted repeatedly from the MS by sweeping the Tx and Rx beams. If the preamble signature is detected, the BS will send an RAR in Step 3. The RAR contains the necessary information for uplink data transmission at the MS, such as TA, temporary identifier, and resource-allocation information. The BS needs to transmit the same RAR repeatedly by sweeping downlink Tx beams because the BS does not yet know the best downlink Tx beam. At this step, the MS knows the best downlink Tx beam pair. Therefore, the RAR is received at the MS with the best downlink Rx beam determined from Step 1. After decoding the RAR, the MS completes uplink synchronization with the BS. In Step 4, the MS transmits the information of the best downlink Tx beam ID, obtained from Step 1, to the BS in a message format after performing a timing adjustment. At this step, the BS determines the best uplink beam pair (uplink Tx beam and Rx beam) using the received message. Note that the best downlink beam pair that is estimated in Step 1 is generally not the same as the best uplink beam pair. In Step 5, the BS sends the information on the best uplink Tx beam ID to the MS. In this step, the downlink message is transmitted using the best downlink Tx beam because the BS has obtained the information from the previous step (Step 4). In Step 6, the MS can send any uplink message using the best uplink Tx beam. Step 6 completes the information exchange (between BS and MS) on the best beam selected for the uplink and downlink. This procedure may be repeated multiple times until successful RA is achieved.

However, the overall RA duration is too long, especially for a moving terminal because the synchronization parameters and best beam pairs need to be reselected periodically. In the proposed procedure, the duration of RA is reduced by transmitting a modified version of the RA preamble used in LTE systems. The proposed RA preamble carries the additional information of the best downlink Tx beam ID at the physical layer as well as preamble signature. The proposed RA procedure is shown in Figure 2. Step 1 in Figure 2 is the same as the first step in the conventional RA procedure. The MS is synchronized with the BS and determines the best downlink beam pair (downlink Tx beam and Rx beam). The MS will select a preamble signature for RA after decoding the SIB transmitted on the best downlink beam pair. In Step 2, the proposed RA preamble is transmitted repeatedly from the MS by sweeping the Tx and Rx beams. The proposed preamble carries the information on the best downlink Tx beam ID and selected preamble ID at the physical layer. Then, the BS detects the best downlink Tx beam ID and preamble ID from the received RA preamble. The BS also determines the best uplink beam pair (uplink Tx beam and Rx beam) from the received preamble. In Step 3, the BS sends an RAR to the MS. The BS does not need to transmit the same RAR repeatedly by sweeping downlink Tx beams because the BS has received the best downlink Tx beam ID from Step 2. The RAR contains the information on the best uplink Tx beam ID as well as the information required for uplink transmission at the MS, such as TA, all at the MAC layer. The RAR is received at the MS with the best downlink Rx beam determined from Step 1. In Step 4, the MS can send any uplink message using the

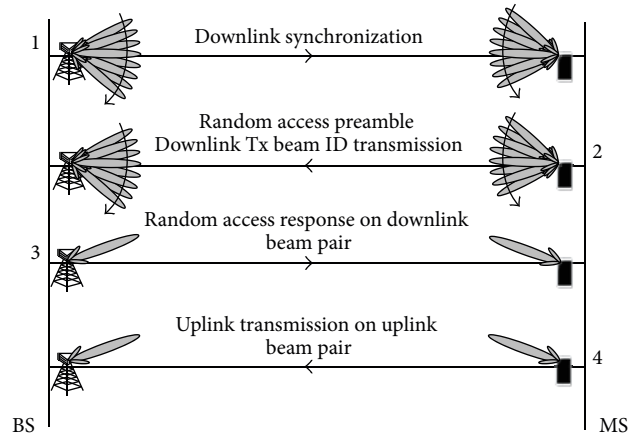


FIGURE 2: Proposed random-access procedure in mm-wave cellular systems.

best uplink Tx beam. In this procedure, the steps required for RA and beam selection are reduced using the proposed RA preamble. In the following sections, we describe the preamble design and detection for RA in mm-wave cellular communication systems with directional beams.

### 3. Proposed RA Preamble

In this section, we discuss an RA preamble that is suitable for mm-wave cellular systems with directional beams. The RA preamble waveform should have good detection probability while maintaining a low false-alarm rate, low collision probability, and low peak-to-average power ratio (PAPR) and allow accurate timing estimation. Because the proposed preamble can be viewed as a modified version of the RAP used in LTE systems, we will start with a short summary on LTE RAP.

The PRACH in LTE systems is generated from the cyclic shift of the prime-length Zadoff-Chu (ZC) sequence, where the root of the sequence is unique to each cell. The 64 different preambles are generated by the cyclic shifts of the base sequence with a length of 839. The MS selects one of 64 available PIDs and transmits the RAP in PRACH [11]. The cyclically shifted ZC sequences have a constant envelope, which ensures low PAPR property. The sequences have an ideal cyclic autocorrelation, which is important for obtaining an accurate timing estimation at the BS. In addition, the cross correlation between different preambles based on the cyclic shifts of the same ZC sequence is zero as long as the cyclic shift is larger than the maximum round-trip propagation delay in the cell plus the maximum delay spread of the channel. Therefore, there is no interference when multiple RA attempts are performed simultaneously using the preambles derived from the same ZC sequence. To handle different cell sizes, the value of the cyclic shift is broadcast as part of the system information. The set of cyclic shifts that produce a zero correlation of the ZC sequence is defined as a zero correlation zone (ZCZ) in the LTE specification [12].

In this paper, we propose two types of RAPs (RAP-1 and RAP-2) for mm-wave cellular communication systems.

The RAP-1 consists of two preambles, each one being constructed with the existing RAP structure in LTE systems. Both preambles share the same root index. The PID and BID are mapped onto cyclic shifts of the first and second preambles, respectively. The best downlink Tx beam ID that is obtained at the MS from Step 1 in the proposed RC procedure will be assigned to the value of BID. Here,  $u$ th root ZC sequence is defined by

$$x_u(n) = e^{-j(\pi un(n+1)/N_{ZC})}, \quad 0 \leq n \leq N_{ZC} - 1, \quad (1)$$

where  $N_{ZC}$  denotes the ZC sequence length. From  $u$ th root ZC sequence, the PID and BID preambles with ZCZ of length  $N_{CS} - 1$  in RAP-1 are defined as follows:

$$x_{1,u}^{b,v}(n) = \{x_{1,u}^v(n), x_{1,u}^b(n)\}, \quad (2)$$

where the two preambles are

$$\begin{aligned} x_{1,u}^v(n) &= x_u((n + C_v) \bmod N_{ZC}), \\ x_{1,u}^b(n) &= x_u((n + C_b) \bmod N_{ZC}) \end{aligned} \quad (3)$$

and cyclic shifts are defined as

$$C_v = \begin{cases} vN_{CS} & v = 0, 1, \dots, \lfloor \frac{N_{ZC}}{N_{CS}} \rfloor - 1, N_{CS} \neq 0 \\ 0 & N_{CS} = 0 \end{cases} \quad (4)$$

$$C_b = \begin{cases} bN_{CS} & b = 0, 1, \dots, \lfloor \frac{N_{ZC}}{N_{CS}} \rfloor - 1, N_{CS} \neq 0, b < N_B \\ 0 & N_{CS} = 0. \end{cases}$$

Here,  $N_{CS}$ ,  $C_v$ ,  $C_b$ , and  $N_B$  denote the length of the cyclic shift in the ZCZ, the cyclic shift mapped onto the PID, the cyclic shift mapped onto the BID, and the number of beams, respectively.  $u, b \in \mathbf{N}_B$ ,  $v \in \mathbf{N}_V$ ,  $\mathbf{N}_B = \{0, 1, \dots, N_B - 1\}$  and  $\mathbf{N}_V = \{0, 1, \dots, \lfloor N_{ZC}/N_{CS} \rfloor\}$  denote the root index uniquely assigned to each cell, BID, PID, set of BIDs, and set of PIDs, respectively. The RAP-1 satisfies the CAZAC property because the structure of the preamble is the same as the RAP in LTE.

The RAP-2 can be viewed as a product of two Chu sequences with different root indices. The first root index is used for cell identification in the same way that the root index in PRACH is used. The BID is mapped onto the second root index. The PID is mapped onto the cyclic shift of the sequence. The RAP-2 is defined as

$$\begin{aligned} x_{2,u}^b(n) &= e^{j(\pi/N_{ZC})(un(n-1)+bn(n+1))}, \\ x_{2,u}^{b,v}(n) &= x_{2,u}^b((n + C_v) \bmod N_{ZC}). \end{aligned} \quad (5)$$

Here, the subscripts 1 and 2 denote RAP-1 and RAP-2, respectively. RAP-2 is designed such that the PID is mapped onto the sequence (with cell ID) in conjunction with its BID. Note that, in RAP-1, the PID is not associated with the BID because they are mapped onto different preambles. The autocorrelation function and frequency-domain version of RAP-2 are given by

$$\begin{aligned} R_{2,u}^b(l) &= \sum_{n=0}^{N_{ZC}-1} x_{2,u}^b(n) [x_{2,u}^b(n+l)]^* \\ &= \sum_{n=0}^{N_{ZC}-1} e^{j(\pi/N_{ZC})(2r_{ub}ln)} e^{j(\pi/N_{ZC})(ul(l-1)+bl(l+1))} \end{aligned} \quad (6)$$

$$= N_{ZC} e^{j(\pi/N_{ZC})(ul(l-1)+bl(l+1))} \delta(\bmod(l, N_{ZC})),$$

$$X_{2,u}^b[k] = x_{r_{ub}}^* [r_{ub}^{-1}k] X_{2,u}^b[0], \quad (7)$$

where

$$X_{2,u}^b[0] = \sqrt{N_{ZC}} \left( \frac{r_{ub}\alpha}{N_{ZC}} \right) \frac{1 - j^{N_{ZC}}}{1 - j} e^{-(j2\pi/N)r_{ub}\alpha\beta^2}, \quad (8)$$

$$r_{ub} = u + b, \quad \alpha = \frac{N_{ZC} + 1}{2}, \quad \beta = \frac{N_{ZC} - 1}{2}.$$

Here,  $r_{ub}^{-1}$  and  $\delta(\cdot)$  denote the multiplicative inverse of  $r_{ub}$  and the Kronecker delta function, respectively.  $(r_{ub}\alpha/N_{ZC})$  denotes the Legendre symbol with a value of  $-1, 1$ , or  $0$ . The frequency-domain version of RAP-2 in (7) can be obtained using the DFT property of the Chu Sequence [13]. The amplitude of the frequency-domain version of RAP-2 is given by  $\sqrt{N_{ZC}}$ , with a constant value for all values of  $n$ . As can be seen from (6), RAP-2 has a zero-autocorrelation property that has a peak amplitude of  $N$  if  $l$  is equal to zero. From (6) and (7), we can see that RAP-2 also satisfies the CAZAC property. However, this property holds only when the root index,  $r_{ub}$ , and sequence length are coprime.

To further analyze the proposed preambles, we examine their correlation properties. The correlation function of the first preamble in RAP-1 is given by

$$\begin{aligned} R_{1,u}(v, v') &= \sum_{n=0}^{N_{ZC}-1} x_{1,u}^v(n) [x_{1,u}^{v'}(n)]^* \\ &= \sum_{n=0}^{N_{ZC}-1} e^{-j(\pi u(n+C_v)(n+C_v+1)/N_{ZC})} e^{j(\pi u(n+C_{v'})(n+C_{v'}+1)/N_{ZC})} \\ &= N_{ZC} e^{j(\pi u(C_{v'}(C_{v'}+1) - C_v(C_v+1))/N_{ZC})} \delta(\bmod(v, v')). \end{aligned} \quad (9)$$

In (9), we observe the interference between preambles when two preambles with PIDs ( $\nu$  and  $\nu'$ ), transmitted from MSs in the same cell, are arrived at the BS. The correlation function of the second preamble in RAP-1 is given by

$$\begin{aligned} R_{1,u}(b, b') &= \sum_{n=0}^{N_{ZC}-1} x_{1,u}^b(n) [x_{1,u}^{b'}(n)]^* \\ &= \sum_{n=0}^{N_{ZC}-1} e^{-j(\pi u(n+C_b)(n+C_b+1)/N_{ZC})} e^{j(\pi u'(n+C_{b'})(n+C_{b'}+1)/N_{ZC})} \\ &= N_{ZC} e^{j(\pi u(C_{b'}(C_{b'}+1)-C_b(C_b+1))/N_{ZC})} \delta(\text{mod}(b, b')). \end{aligned} \quad (10)$$

(10) shows the interference between preambles when two preambles with BIDs ( $b$  and  $b'$ ), transmitted from MSs in the same cell, are arrived at the BS. The results show that the preambles (RAP-1) in the same cell (same root index) are orthogonal, implying that there is no interference when BIDs or PIDs in the same cell are different. When two preambles with PIDs ( $\nu$  and  $\nu'$ ), transmitted from MSs in different cells (different root indices), arrive at the BS, the interference between preambles is given by

$$\begin{aligned} R_{1,u,u'}(\nu, \nu') &= \sum_{n=0}^{N_{ZC}-1} x_{1,u}^\nu(n) [x_{1,u'}^{\nu'}(n)]^* \\ &= \sum_{n=0}^{N_{ZC}-1} e^{-j(\pi \nu(n+C_\nu)(n+C_\nu+1)/N_{ZC})} e^{j(\pi \nu'(n+C_{\nu'})(n+C_{\nu'}+1)/N_{ZC})} \\ &= e^{j(\pi u' C_{\nu'}^2 - u C_\nu^2 - (u' - u)^{-1} (u' C_{\nu'} - u C_\nu)^2 / N_{ZC})} \Sigma_{u,u'}. \end{aligned} \quad (11)$$

When two preambles with BIDs ( $b$  and  $b'$ ), transmitted from MSs in different cells, arrive at the BS, the interference between preambles is given by

$$\begin{aligned} R_{1,u,u'}(b, b') &= \sum_{n=0}^{N_{ZC}-1} x_{1,u}^b(n) [x_{1,u'}^{b'}(n)]^* \\ &= \sum_{n=0}^{N_{ZC}-1} e^{-j(\pi u(n+C_b)(n+C_b+1)/N_{ZC})} e^{j(\pi u'(n+C_{b'})(n+C_{b'}+1)/N_{ZC})} \\ &= e^{j(\pi u' C_{b'}^2 - u C_b^2 - (u' - u)^{-1} (u' C_{b'} - u C_b)^2 / N_{ZC})} \Sigma_{u,u'}, \end{aligned} \quad (12)$$

where

$$\begin{aligned} \Sigma_{u,u'} &= \sqrt{N_{ZC}} \begin{cases} \left( \frac{|(u' - u)|\alpha}{N_{ZC}} \right) \frac{1 - j^{N_{ZC}}}{1 - j} e^{-j(2\pi/N_{ZC})(u' - u)\alpha\beta^2}, & u' > u \\ \left( \frac{|(u' - u)|\alpha}{N_{ZC}} \right) \frac{1 + j^{N_{ZC}}}{1 + j} e^{-j(2\pi/N_{ZC})(u' - u)\alpha\beta^2}, & u' < u, \end{cases} \\ \alpha &= \frac{N_{ZC} + 1}{2}, \quad \beta = \frac{N_{ZC} - 1}{2}. \end{aligned} \quad (13)$$

Equations (11) and (12) are derived using Gauss sum expression [14]. The results show that the preambles (RAP-1), which are transmitted from MSs in different cells, are not orthogonal, and the amplitude of the correlation is given by  $\sqrt{N_{ZC}}$ . In a similar manner, the correlation functions of RAP-2 with different PIDs or BIDs, which are transmitted from MSs in the same cell or different cells, are given by

$$R_{2,u}(\nu, \nu') = \sum_{n=0}^{N_{ZC}-1} x_{2,u}^{b,\nu}(n) [x_{2,u}^{b,\nu'}(n)]^* = N_{ZC} e^{j(\pi/N_{ZC})((C_\nu - C_{\nu'})u(C_\nu + C_{\nu'} - 1))} e^{j(\pi/N_{ZC})((C_\nu - C_{\nu'})b(C_\nu + C_{\nu'} + 1))} \delta(\text{mod}(\nu, \nu')), \quad (14)$$

$$R_{2,u}(b, b') = \sum_{n=0}^{N_{ZC}-1} x_{2,u}^{b,\nu}(n) [x_{2,u}^{b',\nu}(n)]^* = \sum_{n=0}^{N_{ZC}-1} e^{j(\pi/N_{ZC})((b-b')(n+C_\nu)(n+C_\nu+1))} = \begin{cases} N_{ZC}, & b = b' \\ \Sigma^{b,b'}, & b \neq b', \end{cases} \quad (15)$$

$$R_2(u, u') = \sum_{n=0}^{N_{ZC}-1} x_{2,u}^{b,\nu}(n) [x_{2,u'}^{b,\nu'}(n)]^* = \sum_{n=0}^{N_{ZC}-1} e^{j(\pi/N_{ZC})((u-u')(n+C_\nu)(n+C_\nu-1))} = \begin{cases} N_{ZC}, & u = u' \\ \Sigma^{u,u'}, & u \neq u'. \end{cases} \quad (16)$$

The results show that the preambles (RAP-2), which are transmitted from MSs in different cells, are not orthogonal regardless of their BID and PID values, and the amplitude of the correlation is given by  $\sqrt{N_{ZC}}$ . When two preambles (RAP-2) with different BIDs ( $b$  and  $b'$ ) are transmitted from MSs in the same cell, the amplitude of the correlation is given by  $\sqrt{N_{ZC}}$ . However, the preambles (RAP-2) with different PIDs in the same cell are orthogonal, implying that the detection probability at the BS will be high when preambles (RAP-2) with different PIDs are transmitted from MSs in the same cell.

#### 4. Preamble Detection

In this section, we describe a detection technique for RAP in mm-wave cellular systems. As discussed in Step 2 of the proposed RA procedure, the proposed preamble will be transmitted repeatedly from the MS by sweeping Tx and Rx beams. The preamble received at the BS contains the information on the best downlink Tx BID (obtained from Step 1) and PID selected from the MS. The BS needs to detect the BID and PID from the received preambles in multiuser and multicell environments. When the RAPs are received

from multiple MSs in neighboring cells, the received signal at the serving BS with  $b$ th Rx beam is given in the frequency domain as follows:

$$\begin{aligned}
Y_{t,b}^s(k) &= \sum_{i=1}^{N_I} \sum_{m=1}^{N_M} G_{\text{Tx},c}^{i,m} G_{\text{Rx},b} X_{t,u_i,m,c}^{b_{\text{DL}}} (k) H_{c,b}^{i,m}(k) \\
&\quad + W(k) \\
&= \sum_{m=1}^{N_M} G_{\text{Tx},c}^{s,m} G_{\text{Rx},b} X_{t,u_i,m,c}^{b_{\text{DL}}} (k) H_{c,b}^{s,m}(k) \\
&\quad + \sum_{i=1, i \neq s}^{N_I} \sum_{m=1}^{N_M} G_{\text{Tx},c}^{i,m} G_{\text{Rx},b} X_{t,u_i,m,c}^{u_i,m}(k) H_{c,b}^{i,m}(k) \\
&\quad + W(k).
\end{aligned} \tag{17}$$

Here,  $G_{\text{Tx},c}^{i,m}$ ,  $G_{\text{Rx},b}$ , and  $H_{c,b}^{i,m}(k)$  are the Tx beam gain at  $c$ th beam of  $m$ th MS in  $i$ th cell, the Rx beam gain at  $b$ th beam of the BS, and the channel frequency response between the  $c$ th beam of the  $m$ th MS in the  $i$ th cell and the  $b$ th beam of the serving BS,  $s$ , where  $c \in \mathbf{N}_C$ ,  $\mathbf{N}_C = \{0, 1, \dots, N_C - 1\}$ .  $X_{t,u_i,m,c}^{b_{\text{DL}}}$  and  $W(k)$  denote the RAP transmitted from the  $m$ th MS in  $i$ th cell carrying the best TX downlink beam,  $b_{\text{DL}} \in N_B$ , which is transmitted from  $c$ th MS beam and additive white Gaussian noise (AWGN) at  $k$ th subcarrier, respectively. Further,  $u_{i,m}$  and  $u_{s,m}$  denote Chu's root indices of  $i$ th cell and serving cell for  $m$ th MS, respectively.  $N_M$  and  $N_I$  denote the number of MSs and neighboring cells, respectively.  $t = \{1, 2\}$  denotes the type of proposed RAP. The received signal can be classified as two parts: the signal received from MSs in the serving cell and interference signals from MSs in neighboring cells.

The preamble-detection process at the BS is composed of a power-delay profile (PDP) computation and signature detection. The PDP computation of the received signal with a specific beam is given by

$$\left| z_{t,u}^{b,v}(l) \right|^2 = \left| \sum_{n=0}^{N_{\text{ZC}}-1} y(n) \left[ x_{t,u}^{b,v}(n+l) \right]^* \right|^2, \quad t = 1, 2, \tag{18}$$

where  $z_{t,u}^{b,v}(l)$  represents the correlation function between the received signal  $y(n)$  and reference RAP  $x_{t,u}^{b,v}(n)$  with lag  $l$ . In (18), the variables for Tx and Rx beams are not included for notational simplicity. The signature detection is made by searching the PDP peaks above a detection threshold over a search window corresponding to the cell size. The detection threshold is determined by the false-alarm probability. From the PDP peaks, the PID and TA can be computed as

$$\text{PID} = \left\lfloor \frac{N_{\text{peak}}}{N_{\text{CS}}} \right\rfloor + 1, \tag{19}$$

$$\text{TA} = \text{mod}(N_{\text{peak}}, N_{\text{CS}}) - 1,$$

where  $N_{\text{peak}}$  denotes the position of the PDP peak. The preamble detection can be performed in the frequency

domain, as shown in Figure 3. First, the received signals are demapped onto the corresponding subcarriers in the frequency domain. Next, the known preamble sequences (RAP-1 or RAP-2) in the time domain are converted to the frequency domain using a discrete Fourier transform (DFT) operation. After multiplication of these two signals, the result is transformed to the time domain by inverse DFT (IDFT). Then, the PID and BID are detected using the PDP in the time domain.

A preamble transmission is detected if the PDP peak is greater than the detection threshold. This process will be performed repeatedly for each Tx-Rx beam pair after evaluating the PDP of each Tx-Rx beam pair with the known RAP. Finally, the BID is detected as

$$\bar{b} = \begin{cases} \arg \max_{b \in N_B} \left| z_{t,u}^{b,v}(l) \right|^2 \\ \arg \max_{b \in N_B} \left| z_{t,u}^{b,v}(l) \right|^2. \end{cases} \tag{20}$$

The preamble-detection probability depends on the detection threshold setting. In LTE systems, the detection threshold is determined by the target false-alarm probability [15, 16]. Here, the false-alarm probability is defined as the probability that the receiver detects a preamble transmission when the received signal is purely noise. When there is no preamble transmission, the PDP of the received signal follows a central chi-square distribution with two degrees of freedom (DoFs), with the mean given by the noise-floor level. The false-alarm probability can be easily obtained from the cumulative distribution function (CDF) by changing the threshold value. Then, the detection threshold can be found by setting the target false-alarm probability. The false-alarm probability for an LTE system with multiple antennas can be derived by accumulating PDPs obtained from multiple antennas. The detection probability can be found using the detection threshold obtained from the false-alarm probability. Here, the detection probability is defined as the probability that the receiver correctly detects the RAP transmitted from the MS. When the proposed RAP is received in mm-wave cellular systems with directional beams, the false-alarm probability in an AWGN channel is given by [15, 16]

$$P_t^{\text{FA}} = \left[ 1 - \left[ \left( 1 - e^{-T_r} \sum_{b=0}^{N_B-1} \frac{1}{b!} (T_r)^b \right)^{N_{\text{ZC}}} \right]^{N_M} \right]^n, \tag{21}$$

where

$$n = \begin{cases} 2 & \text{if } t = 1 \\ 1 & \text{if } t = 2. \end{cases} \tag{22}$$

Here,  $T_r$  denotes the threshold value normalized by the noise-floor level. The false-alarm probabilities are given for the cases of RAP-1 and RAP-2. Note that, in the cases of RAP-1 consisting of two symbols, the false-alarm probabilities of PID and BID are multiplied to obtain the total false-alarm probability. From (21), we can obtain the plot of the false-alarm probability by changing the threshold value. From

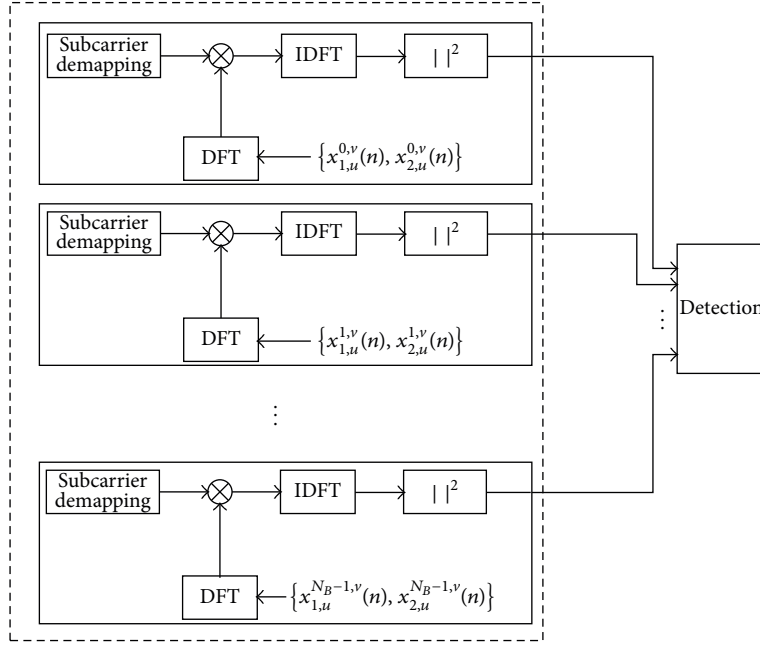


FIGURE 3: Detection process of proposed preamble.

the plot, we determine the detection threshold by setting the target false-alarm probability. Using the value of the detection threshold, the detection probabilities of RAP-1 and RAP-2 can be obtained as [15, 16]

$$P_1^D = \left(1 - \frac{1}{N_B}\right)^{N_{\text{MS}}-1} [Q_1(\sqrt{\delta}, \sqrt{\lambda})]^2, \quad (23)$$

$$P_2^D = Q_1(\sqrt{\delta}, \sqrt{\lambda}),$$

where  $\delta$  and  $\lambda$  denote the noncentrality parameter and detection threshold, respectively.  $Q_n(\cdot)$  represents the Marcum Q-function. The performance of the proposed RAP in mm-wave cellular systems with beamforming can be evaluated using the false-alarm probability and detection-probability functions.

## 5. Simulation

We evaluated the performance of the proposed RAP by performing computer simulations using a simple model of a mm-wave cellular system with directional beams. Before applying the proposed RAP to the mm-wave cellular system, we verified the properties of the proposed RAP described in Section 2. Figures 4 and 5 show the correlation properties of RAP-1 and RAP-2, respectively. Here, we assumed that the sequence length is 839, and the PID and BID of MS1 under the test are set to 44 and 2, respectively. The values of the PID and BID of MS2 are assumed to vary. Scenario 1 refers to the case where two MSs (MS1 and MS2) are located in the serving cell. In Scenario 2, it is assumed that MS1 is located in the serving cell and MS2 is located in the neighboring cell. As can be seen from Figure 4(a), the correlation value of RAP-1 in Scenario 1 is zero, with the exception of the case where MS2 has the same PID = 44. In this case, the magnitude of

the correlation becomes 839 ( $N_{ZC}$ ), as given by (9). As can be seen from Figure 4(b), we can obtain the same result, with the exception of the case where  $\text{BID} = 2$ , as given by (10). However, the correlation value of RAP-1 in Scenario 2 is 28.97 ( $\sqrt{N_{ZC}}$ ) for all values of PID and BID, as given by (11) and (12), respectively. We can confirm this result from Figures 4(a) and 4(b). As can be seen from Figure 5(a), the correlation value of RAP-2 in Scenario 1 is zero, except for the case where MS2 has the same PID = 44. In this case, the magnitude of the correlation becomes 839, as given by (14). As can be seen from Figure 5(b), the correlation value of RAP-2 in Scenario 1 becomes 839 only when we use the same value of BID (2). However, the correlation value becomes 28.97 when we use another value of BID, as given by (15). The correlation value of RAP-2 in Scenario 2 is 28.97 for all values of PID and BID, as given by (16).

Figures 6(a) and 6(b) show false-alarm probabilities of RAP-1 and RAP-2, respectively. We obtain the false-alarm probability using both the analytic solution in (21) and the simulation when the number of MSs varies. The PDP received at the BS is compared to the normalized threshold value, which varies from 10 to 30. The threshold value for preamble detection, which satisfies the required false-alarm probability, can be found from Figure 6. The value of the false-alarm probability is set to be less than 0.1%, as in LTE systems. As can also be seen in Figure 6, the threshold value satisfying the required false-alarm probability is sensitive to the number of users in the cell. The threshold value needs to be increased to avoid the misdetection of RAP as the number of MSs increases. We also see that the simulation results agree well with the analytical results in (21). From these results, we determined the threshold values for the detection probability as follows: 22 for 1 MS, 24 for 3 MSs, and 26 for 5 MSs in the case

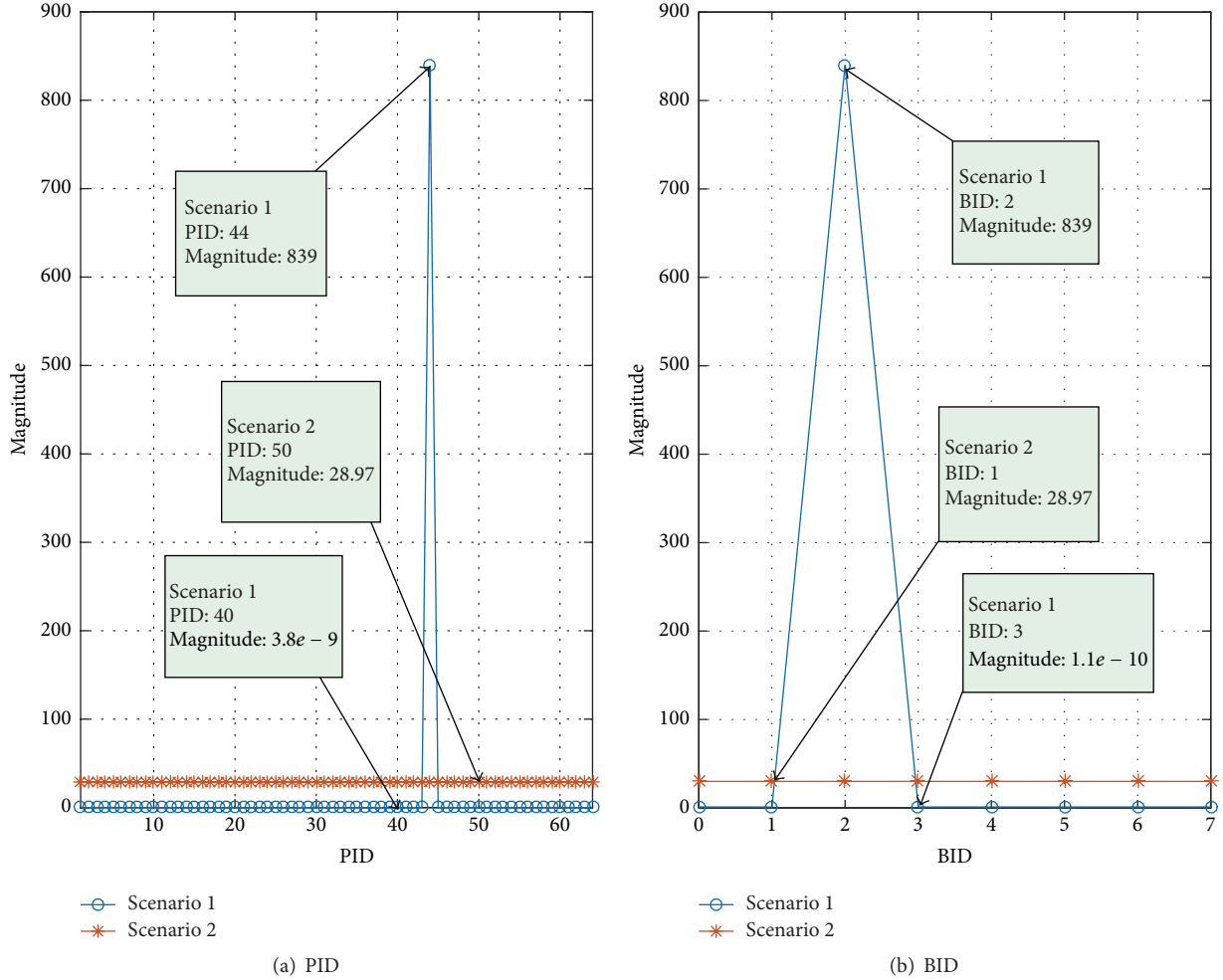


FIGURE 4: Correlation property of RAP-1.

of RAP-1, and 26 for 1 MS, 30 for 3 MSs, and 38 for 5 MSs in the case of RAP-2.

Figures 7(a) and 7(b) show the detection probabilities of RAP-1 and RAP-2, respectively. The threshold values selected for the previous results are used for preamble detection. For the simulation, we used a three-dimensional spatial channel model (3D SCM), which is often used for the system simulation of cellular systems, with the SNR varying from  $-40$  to  $-18$  dB with a step size of 2 dB. We set the carrier frequency, subcarrier spacing, and FFT size to 28 GHz, 270 KHz, and 2048, respectively. The number of antenna elements is 16 at both the BS and MS, all with a uniform rectangular array (URA). The positions of the MSs are randomly placed in a cell, and the best Tx-Rx beam directions are derived from their respective positions. PIDs are assigned as [40 44 26 17 10] when the number of MSs is five. As can be seen from Figure 7, the detection probability tends to degrade as the number of MSs increases. That is because of the increased interference as the number of RAPs received at the BS increases.

However, the detection probability of RAP-1 in Figure 7(a) degrades more significantly compared with that

of RAP-2. In the case of RAP-1, the detection probability cannot reach 100%, even in high SNR regions when the number of MSs is larger than three. This may result in system failure because of the misdetection of the PID or BID. This phenomenon results from the structure of RAP-1 being composed of two preambles. Because the PID and BID are detected separately, it is difficult to determine the relationship between the detected PID and BID. It is not possible to know whether the detected PID and BID are from the same source (MS) in the case of RAP-1. On the other hand, the detection probability of RAP-2 in Figure 7(b) is 100% in higher SNR regions when the number of MSs is five. This is because the PID and BID in RAP-2 are related to each other. Once the preamble is detected, the PID and BID are found simultaneously in the case of RAP-2. From Figure 7, it can also be seen that simulation results agree well with the analytical results in (23). From these results, we can see that the RAP-2 is appropriate for the detection of RAP in multiuser environments.

Table 1 compares the processing time and number of complex multiplications when we used the conventional and proposed RA procedures. Here, we excluded the downlink



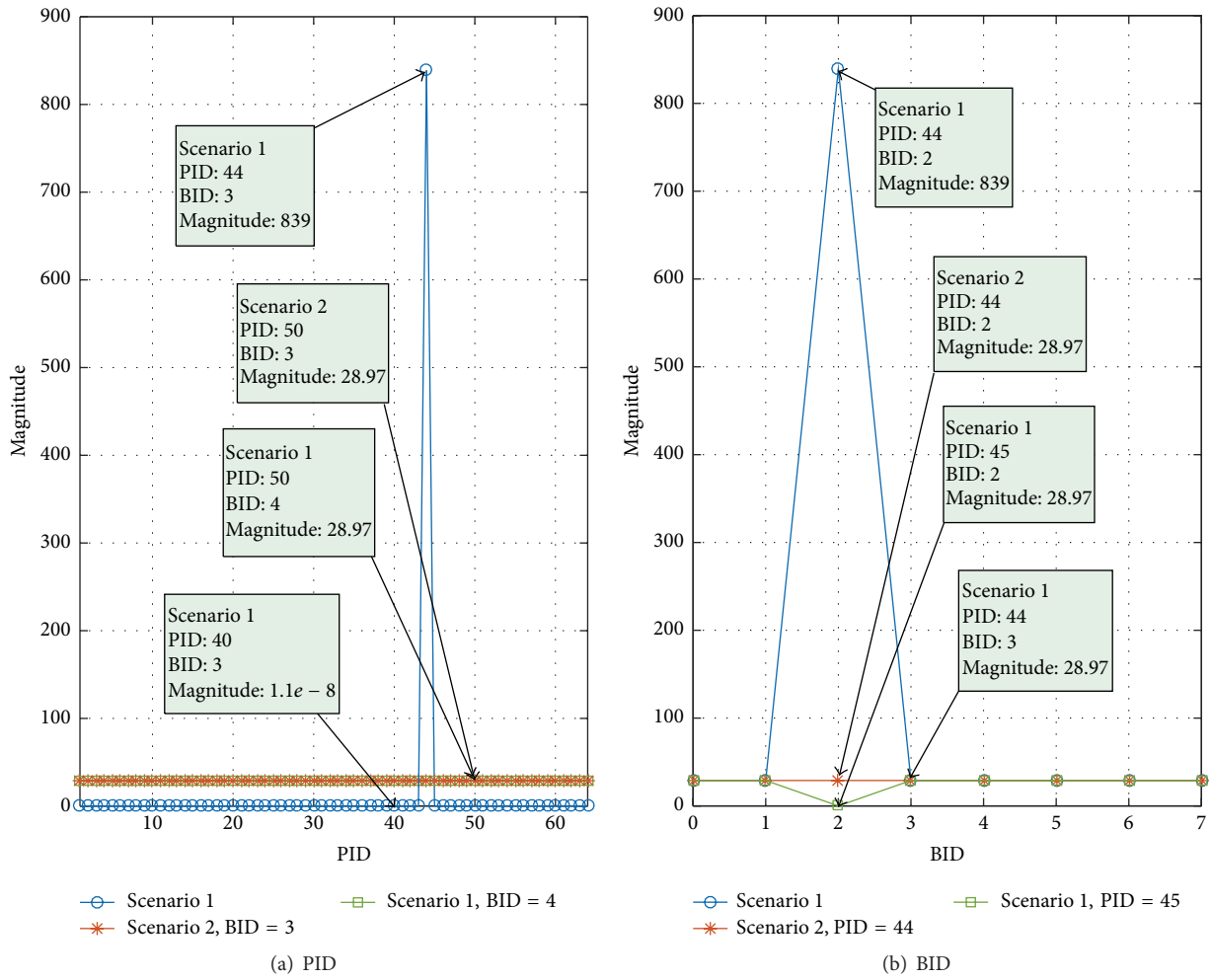


FIGURE 5: Correlation property of RAP-2.

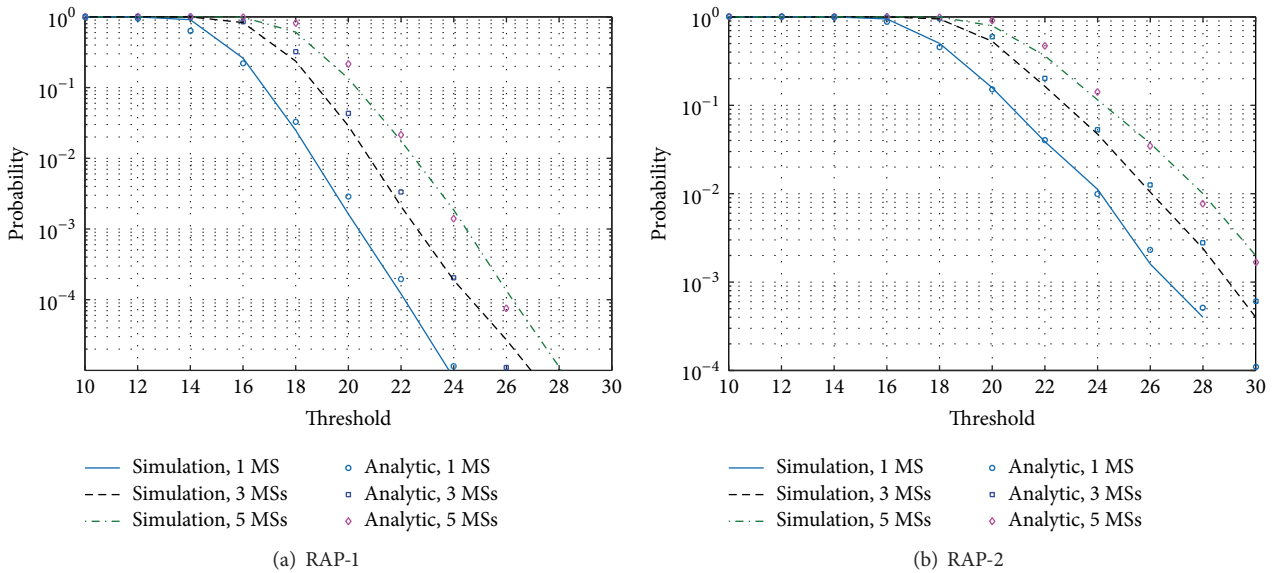


FIGURE 6: False-alarm probabilities of RAP-1 and RAP-2.

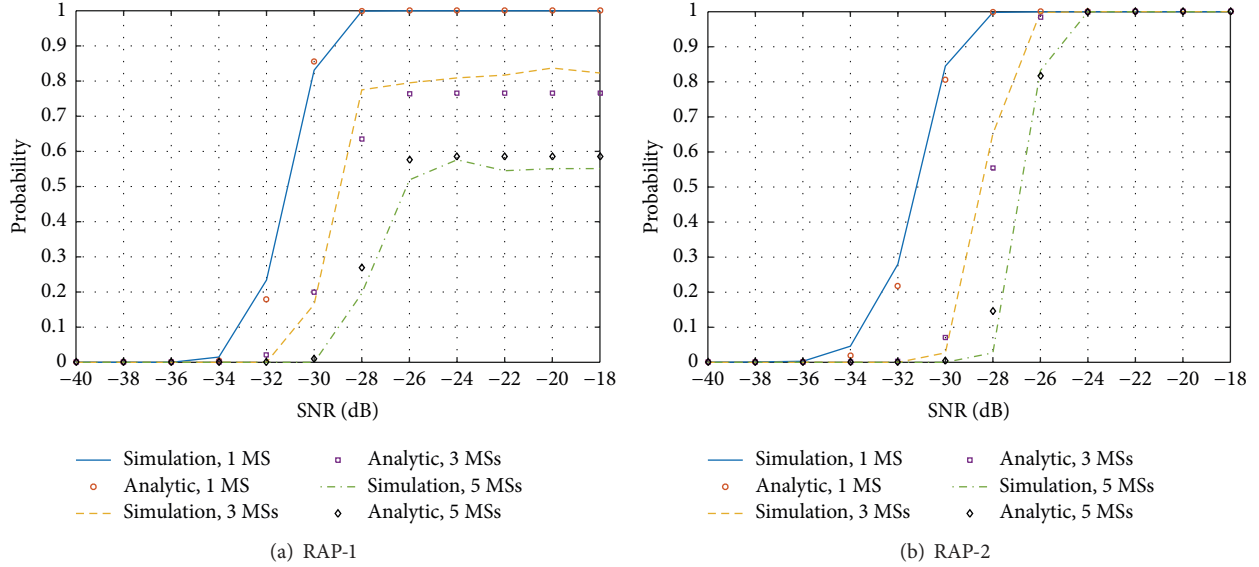


FIGURE 7: Detection probabilities of RAP-1 and RAP-2.

TABLE 1: Comparison of conventional and proposed RA procedures.

Item	Conventional RA procedure	Proposed RA procedure	
		RAP-1	RAP-2
Processing time ( $\mu s$ )	$T_{\text{RAP}} \cdot (2 \cdot N_B \cdot N_C + N_B)$ (108, 800)	$2 \cdot T_{\text{RAP}} \cdot (N_B \cdot N_C)$ (102, 400)	$T_{\text{RAP}} \cdot (N_B \cdot N_C)$ (51, 200)
Number of complex multiplications	$N_B \cdot N_C \cdot N_{\text{ZC}}^2$ (45, 050, 944)	$2 \cdot N_B \cdot N_C \cdot N_{\text{ZC}}^2$ (90, 101, 888)	$N_B \cdot N_C \cdot N_{\text{ZC}}^2$ (45, 050, 944)

synchronization step (Step 1) because this step is common to both procedures. In addition, we do not consider the steps that do not require beam sweeping (Step 5 and Step 6 in the conventional RA procedure, and Step 3 and Step 4 in the proposed RA procedure) because the processing time and complexity are minimal. In the conventional RA procedure, the processing time required for Step 2 and Step 4 is given by the product of the number of BS beams ( $N_B$ ) and the number of MS beams ( $N_C$ ). In addition, the processing time required for Step 3 is given by the number of BS beams. For the proposed RA procedure, the processing time required for Step 2 is given by the product of the number of BS beams and the number of MS beams. Here, an example is shown in parenthesis when  $N_B = 8$  and  $N_C = 8$ . The RAP duration  $T_{\text{RAP}}$  is assumed to be  $800 \mu s$ , as in LTE systems. As can be seen in Table 1, the RAP-1 requires twice the processing time when compared to RAP-2 because two sequences are used in RAP-1. Note that RAP-2 requires half of the processing time when compared with the conventional technique. Next, we compared the computational complexities required for preamble detection. In order to detect the RAP, we require complex multiplications equal to  $N_{\text{ZC}}^2$  for a correlator with the size of  $N_{\text{ZC}}$ . The total number of complex multiplications required for preamble detection in Step 2 (conventional technique and RAP-2) is given by  $N_B \cdot N_C \cdot N_{\text{ZC}}^2$  because the detection process needs to be performed in all directions.

The number of complex multiplications required for the RAP-1 is twice that of the conventional one because the RAP-1 uses two preambles.

## 6. Conclusion

In this paper, we proposed two different types of preambles (RAP-1 and RAP-2) to reduce the processing time required for RA in mm-wave cellular systems with directional beams. Using simulations, we showed that the proposed RA procedure with the preamble (RAP-1 or RAP-2) can reduce the processing time, compared with the conventional RA procedure. However, in the case of RAP-1, the detection probability decreases significantly as the number of MSs increases, because the PID and BID are detected separately. In the case of RAP-2, a 100% detection probability can be achieved in high SNR regions even when the number of MSs is five, because the PID in RAP-2 is designed in association with the BID. Also, 6% and 53% reduction gains in processing time can be obtained when RAP-1 and RAP-2 are used, respectively. Hence, the RAP-2 was shown to be better suited for RA in mm-wave cellular systems with directional beams because of the shorter processing time, high detection probability in multiuser environments, and reasonable computational complexity (similar to the conventional one).

## Competing Interests


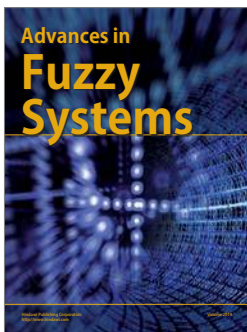
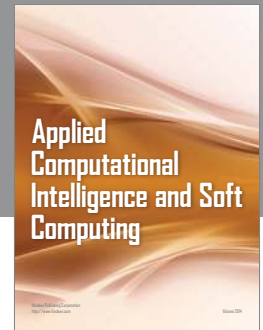
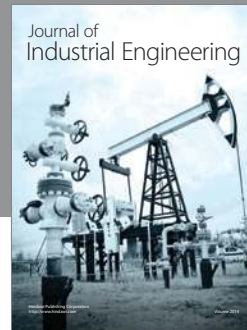
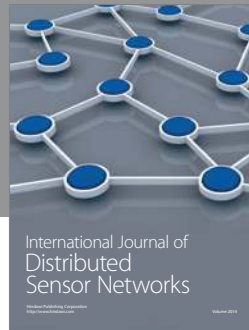
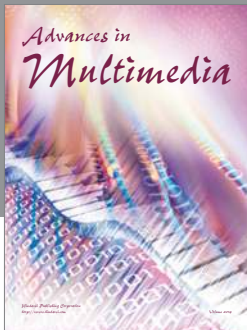
The authors declare that there is no conflict of interests regarding the publication of this paper.

## Acknowledgments

This research was supported by the MSIP (Ministry of Science, ICT and Future Planning), Korea, under the ITRC (Information Technology Research Center) support program (IITP-2016-H8501-15-1007) supervised by the IITP (Institute for Information & Communications Technology Promotion) and Basic Science Research Program through the National Research Foundation of Korea (NRF) funded by the Ministry of Education (2015R1D1A1A01057628).

## References

- [1] S. Rangan, T. S. Rappaport, and E. Erkip, "Millimeter-wave cellular wireless networks: potentials and challenges," *Proceedings of the IEEE*, vol. 102, no. 3, pp. 366–385, 2014.
- [2] T. S. Rappaport, F. Gutierrez, E. Ben-Dor, J. N. Murdock, Y. Qiao, and J. I. Tamir, "Broadband millimeter-wave propagation measurements and models using adaptive-beam antennas for outdoor Urban cellular communications," *IEEE Transactions on Antennas and Propagation*, vol. 61, no. 4, pp. 1850–1859, 2013.
- [3] W. Hong, K.-H. Baek, Y. Lee, Y. Kim, and S.-T. Ko, "Study and prototyping of practically large-scale mmWave antenna systems for 5G cellular devices," *IEEE Communications Magazine*, vol. 52, no. 9, pp. 63–69, 2014.
- [4] M. Bennis, S. M. Perlaza, P. Blasco, Z. Han, and H. V. Poor, "Self-organization in small cell networks: a reinforcement learning approach," *IEEE Transactions on Wireless Communications*, vol. 12, no. 7, pp. 3202–3212, 2013.
- [5] A. T. Nassar, A. I. Sulyman, and A. Alsanie, "Radio capacity estimation for millimeter wave 5G cellular networks using narrow beamwidth antennas at the base stations," *International Journal of Antennas and Propagation*, vol. 2015, Article ID 878614, 6 pages, 2015.
- [6] B. Li, Z. Zhou, H. Zhang, and A. Nallanathan, "Efficient beam-forming training for 60-GHz millimeter-wave communications: a novel numerical optimization framework," *IEEE Transactions on Vehicular Technology*, vol. 63, no. 2, pp. 703–717, 2014.
- [7] S. K. Yong, P. Xia, and A. Valdes-Garcia, *60 GHz Technology for Gbps WLAN and WPAN: From Theory to Practice*, John Wiley & Sons, New York, NY, USA, 2011.
- [8] C. Jeong, J. Park, and H. Yu, "Random access in millimeter-wave beamforming cellular networks: issues and approaches," *IEEE Communications Magazine*, vol. 53, no. 1, pp. 180–185, 2015.
- [9] M. Lott, "Adaptive random access with beam-forming in 4G mobile networks," in *Proceedings of the IEEE 63rd Vehicular Technology Conference (VTC-Spring '06)*, pp. 435–439, Melbourne, Australia, July 2006.
- [10] E. Dahlman, S. Parkvall, and J. Skold, *4G LTE/LTE-Advanced for Mobile Broadband*, Elsevier, Oxford, UK, 2011.
- [11] S. Sesia, I. Toufik, and M. Baker, *LTE—The UMTS Long Term Evolution: From Theory to Practice*, John Wiley & Sons, Chichester, UK, 2011.
- [12] LTE Standard, *LTE; Evolved Universal Terrestrial Radio Access (EUTRA); Physical Channels and Modulation (3GPP TS 36.211 Version 12.6.0 Release 12)*, 2015.
- [13] B. M. Popovic, "Efficient DFT of Zadoff-Chu sequences," *Electronics Letters*, vol. 46, no. 7, pp. 502–503, 2010.
- [14] B. C. Berndt, R. J. Evans, and K. S. Williams, *Gauss and Jacobi Sums*, Canadian Mathematical Society Series of Monographs and Advanced Texts, John Wiley & Sons, New York, NY, USA, 1998.
- [15] O. Altrad and S. Muhaidat, "A new mathematical analysis of the probability of detection in cognitive radio over fading channels," *EURASIP Journal on Wireless Communications and Networking*, vol. 2013, no. 1, article 159, 11 pages, 2013.
- [16] K. Simon, *Probability Distribution Involving Gaussian Random Variables: A Handbook for Engineers and Scientists*, Springer, Berlin, Germany, 2002.



**Hindawi**

Submit your manuscripts at  
<http://www.hindawi.com>

